Journal of Applied Physics

Chain substitution caused sub-fibril level differences in electromechanical structure and property of wild-type and oim/oim collagen fibers

Cite as: J. Appl. Phys. **128**, 235111 (2020); https://doi.org/10.1063/5.0016535
Submitted: 07 June 2020 . Accepted: 17 November 2020 . Published Online: 21 December 2020

Yao Sun, Tao Li, Qiaomei Sun, Yuan Cheng, and Kaiyang Zeng

Journal of Applied Physics ARTICLE scitation.org/journal/jap

Chain substitution caused sub-fibril level differences in electromechanical structure and property of wild-type and oim/oim collagen fibers

Cite as: J. Appl. Phys. **128**, 235111 (2020); doi: 10.1063/5.0016535
Submitted: 7 June 2020 · Accepted: 17 November 2020 ·
Published Online: 21 December 2020

Yao Sun,[1,2] Tao Li,[3] Qiaomei Sun,[1] Yuan Cheng,[4,a)] and Kaiyang Zeng[1,a)]

AFFILIATIONS

[1]Department of Mechanical Engineering, National University of Singapore, Singapore
[2]School of Science, Harbin Institute of Technology, Shenzhen 518055, People's Republic of China
[3]Center for Spintronics and Quantum System, State Key Laboratory for Mechanical Behavior of Materials, School of Materials Science and Engineering, Xi'an Jiaotong University, Xi'an, Shaanxi Province 710049, People's Republic of China
[4]Institute of High-Performance Computing, Agency for Science Technology and Research, 1 Fusionopolis Way, Singapore 138632

[a)]**Authors to whom correspondence should be addressed:** chengy@ihpc.a-star.edu.sg and mpezk@nus.edu.sg

ABSTRACT

Electromechanical changes in type I collagen caused by diseases are pivotal for monitoring bone health and offering informative message of constructing biobased smart devices. Here, we employ a mouse model of osteogenesis imperfecta (oim/oim), which is genetically modified through mutating the α-2 chain to α-1 chain in the collagen fibrils of the wild-type model (+/+ or heterotrimer), resulting in three α-1 chains in the collagen fibrils (i.e., homotrimer). Piezoresponse force microscopy (PFM) is used to directly visualize the sub-micrometer structures and piezoresponses of +/+ and oim/oim collagen fibers. Results show that the compact and highly ordered +/+ collagen fibers possess larger in-plane piezoresponses than the loosely packed and randomly distributed oim/oim collagen fibers. The mean values of the lateral PFM amplitude are 108.53 pm and 77.72 pm with interquartile ranges of 98.56–117.47 pm and 71.21–85.93 pm for +/+ and oim/oim collagen fibers, respectively. Molecular simulations demonstrate that the structural stability and electrically induced activity of heterotrimer are better than those of homotrimer, suggesting better biopiezoelectricity of comprising diverse polar residues (atomic charges) within the oriented heterotrimeric collagen molecular structure. Our study provides a new insight into the functional changes of human osteogenesis imperfecta.

I. INTRODUCTION

Biopiezoresponse is a type of electromechanical coupling phenomenon in bio-organic molecular nanostructures.[1] Up to now, the biopiezoelectricity has been explored in a large number of biomaterials, including proteins, biopolymers, molecular systems, polysaccharides, organelles, glands, and seashells.[1–9] One of the most studied biomaterials, bone, is mainly composed of strongly aligned polar organic type I collagen molecules embedded in the inorganic matrix of mineral.[10] Many results have showed that the piezoelectric effect can promote bone growth, repair, construction, while even being suitable for bone tissue engineering.[11–15] In particular, the fibril-forming type I collagen has a crucial role in maintaining the structural integrity and functional properties of the bones.[16] The typical hierarchical structure of type I collagen can be subdivided into six levels at nano- to sub-microscales (Fig. 1). At level 1, individual amino acid residues form G-X-Y triplets,[17] whereas the X and Y can be any amino acid residues and G is glycine. Level 2 consists of thousands of amino acids that are bonded together in the form of $-[G\text{-}X\text{-}Y]_n-$ to construct a long α chain through peptide bonds (amide bonds).[18] At level 3, the α chains are produced in two forms, namely, α-1 and α-2,[19] by different genes encoding. α-1 and α-2 chains have different compositions of amino acids and sequences. The wild-type type I collagen has a heterotrimeric form consisting of two α-1 chains and one α-2 chain, while certain type I collagen in fetal tissues, fibrosis, and cancer in humans has a homotrimeric form which consists of three α-1 chains,[20] i.e., α-2 chain is replaced by α-1 chain in those

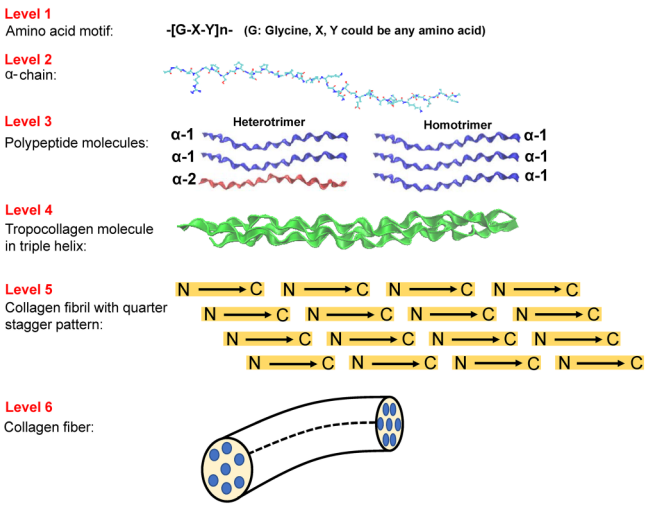

FIG. 1. Schematics of the hierarchical structures of collagen fibers in +/+ heterotrimer and oim/oim homotrimer, showing the detailed sequences of the six levels. At level 1, individual amino acid residues form G-X-Y triplets, whereas X and Y can be any amino acid residues and G is glycine. At level 2, thousands of amino acids bond in the form of -[G-X-Y]$_n$- to form a long α chain through peptide bonds. At level 3, three α chains are produced in a collagen molecule. The wild-type type I collagen molecule has a heterotrimeric form consisting of two α-1 chains and one α-2 chain. Type I collagen molecules in fetal tissues, fibrosis, and cancer in humans have homotrimeric forms, which consist of three α-1 chains. At level 4, three left-handed α chains join together to form a right-handed triple helical tropocollagen. At level 5, tropocollagens form larger collagen aggregates in a stagger pattern so that the collagen fibril has a polar orientation directed from the amine N-terminus (ACE) to the carboxyl C-terminus (NME). At level 6, collagen fibrils embed in the mineral matrix to form the mineralized collagen fibers.

diseased collagens. At level 4, three left-handed α chains join together to form a right-handed triple helical tropocollagen.[21] At level 5, tropocollagens form larger collagen aggregates in a stagger pattern so that the collagen fibril has a polar orientation directed from the amine N-terminus (ACE) to the carboxyl C-terminus (NME).[22] At level 6, collagen fibrils embed in the mineral matrix to form the mineralized collagen fibers.[23]

Biopiezoelectricity of bone was first discovered by Fukada and Yasuda in 1957.[24] They proposed that its piezoelectricity was ascribed to the crystalline micelles of the collagen molecules. Subsequently, a large amount of studies have been devoted to unraveling the origin of piezoelectricity in bones[10,25–29] and fibril-forming collagens.[30–34] In 1981, Hastings *et al.* reported the bioferroelectricity of dry cortical bone since its polarization vs electric field (P–E) relationship was comparable to that of the weak ferroelectric materials and it could be characterized by a hysteresis loop.[35] However, the results of bioferroelectricity on moist bone were unreliable because of the leakage currents.[36] Over the past decade, the studies on piezoelectricity in bone and collagen fibrils have come into the era of nanometer precision. This is due to the development of atomic force microscopy (AFM) based techniques making the probing of multi-properties in these complex materials at nanoscale feasible. Piezoresponse force microscopy (PFM) has been well developed to characterize the nanoscale piezoelectricity of various materials, including semiconductors,[37,38] organic polymers,[39,40] and biological samples.[23,41–55] As for collagen, dozens of papers have been devoted to using PFM to characterize its nanoscale piezoelectricity. Harnagea *et al.* realized the 2D nanoscale mapping of the electromechanical behavior of individual type I collagen fibril and found that shear piezoelectric activity was associated with piezoelectric deformation along the long axis of the fibril.[56] Minary-Jolandan *et al.* also reported that single collagen fibril could behave predominantly as shear piezoelectric materials with a piezoelectric coefficient of 1 pm/V.[57] Additionally, they proposed that there existed an intrinsic piezoelectric heterogeneity within a collagen fibril coinciding with the periodic variation of its gap and overlap regions.[58] Jiang *et al.* recently published a work to resolve the complex heterogeneity and intrinsic fine electromechanical structure of collagen by sequential excitation PFM which excited the electromechanical response of collagen via a sequence of distinct frequencies to minimize the crosstalk with topography.[59] They found that the gap and overlap regions of collagen fibers exhibited different electromechanical amplitudes. Except for the continuously burgeoning PFM, molecular simulation stays always a powerful tool for the detailed analysis of correlation between the structural–mechanical/piezoelectric properties of protein or other bio-inspired materials.[60–64] However, the current literature is still lacking a good simulation explanation of electric induced behaviors of α chain and aggregates in the bone.[65–67]

Osteogenesis imperfecta (OI), also known as a brittle bone disease, is one of the genetic disorders that has adverse effects on the bone health and has no cure currently.[68] The underlying mechanism is usually the problems of connective tissues due to a lack of type I collagen.[69] In more than 90% of such cases, mutations in the α-1 or α-2 genes occurred.[69,70] Osteogenesis imperfecta murine (oim) is a mouse model with well-defined genetic mutation,[71] and it was widely used to study the OI mechanisms. It was believed that the observations of abnormal mineral alignments with respect to collagens in the oim model are consistent with those reported in human OI.[71] It was also found that the collagen in the oim bone was easily kinked and rotated with larger angles than those in the wild-type bone.[20] In addition, for the wild-type bone, the collagen fibrils have higher mechanical strength than those of the oim bone, as well as the overall mechanical properties.[20,72–75] Despite a handful of theoretical and experimental works that have addressed the morphological changes[76] as well as mechanical strength differences between the wild-type and oim bones, it still remains unclear that what are the differences in the electromechanical coupling behaviors between the two as well as how this coupling contributes toward the mechanisms and treatments of brittle bone disease.

In this work, mouse model (oim/oim) with alteration in type I collagen, i.e., mutating the α-2 chain to α-1 chain in tropocollagen molecule, was adopted to study the biopiezoelectricity of brittle bone for the first time. The controlled (wild-type) group +/+ was used as a reference and counterpart. The in-plane and out-of-plane piezoelectric responses of collagen fibers from the two groups' bone samples were mapped *via* lateral PFM (LPFM) and vertical PFM (VPFM), respectively. Furthermore, molecular dynamics simulations were performed to compare the in-plane and out-of-plane

responses of the two collagen models under specific electric fields. A homotrimeric isoform simulation model consisting of three α-1 chains was used to mock the type I collagen in the oim/oim bone, and a heterotrimeric model consisting of two α-1 chains and one α-2 chain was used to mimic the type I collagen in the +/+ bone. The field emission scanning electron microscopy (FESEM) and energy dispersive x-ray spectroscopy (EDS) experiments were adopted to reveal the morphology and chemistry changes between +/+ and oim/oim collagen fibers. Through the experimental and simulation works, we have found that the α-2 chain can improve the piezoresponse of collagen fibrils. Specifically, the stronger piezoelectricity can be achieved by forming heterotrimeric peptide chains comprising versatile polar residues with versatile atomic charges in the oriented structure of the collagen biomacromolecules.

II. MATERIALS AND METHODS

A. Mouse model and sample preparation

The mouse model is a type of B6C3Fe-a/aCol1a2oim/oim strain (oim/oim) that replicates the moderate to severe condition of human OI.[75] Humeri of the 8 weeks old female mouse bones (for both oim/oim and +/+ groups) were cleaned up and subsequently dried in air for an hour. The dried bone samples were then embedded in epoxy resin (EPOTHIN, Buehler, Lake Bluff, USA) and polymerized at room temperature. After polymerization, the resin-cast bone samples were cut into cubes using a diamond saw (Isomet, Buehler GmbH, Germany). Afterward, the bone samples were polished using carbide papers (from P800 to P4000) and alumina powders (0.3 μm and 0.05 μm) to achieve the mirror-like surfaces for PFM studies. The PFM experiments were conducted under ambient air condition with a relative humidity of 50%–60% and room temperature (~25 °C).

B. Piezoresponse measured by PFM

PFM imaging was conducted on a commercial Scanning Probe Microscope (MFP-3D, Asylum Research, Oxford Instruments, Santa Barbara, USA). The conductive probes (PPP-CONTSCPt, Nanosensors, Switzerland and PPP-CONTPt-50, Nanosensors, Switzerland) (Tables S1 and S2 in the supplementary material) were used in the PFM experiments for both +/+ and oim/oim collagen fibers. LPFM calibration was undertaken according to the geometry of the cantilever using the equation $R = 2L/3h$, where L is the length of the cantilever, h is the combined height of the tip and cantilever thickness, and R is the ratio between the out-of-plane sensitivity and the in-plane sensitivity. VPFM calibration was undertaken using Sader and thermal noise methods before all imaging. The scan angle of 90° is adopted for all the PFM experiments. An AC bias of 3 V_{peak} was supplied *via* the conductive probe that was in contact with the sample to induce the sample oscillation according to the inverse piezoelectricity. Because of the weak piezoresponse of the biomaterials, resonance enhancement technique was applied. Both amplitude and phase images were acquired near the contact resonance, which revealed the information of bias-induced deformation and polarization orientation, respectively. To acquire the in-plane and out-of-plane piezoresponses, LPFM and VPFM were used, by which the shear and normal strain of the collagen fibers were recorded, respectively, upon an application of a vertical electric bias. The LPFM and VPFM experiments were conducted on multiple +/+ and oim/oim samples and multiple locations at each sample. For each probe, the samples from the two models were alternately scanned. Amplitude values of thirty (30) collagen fibers from 10 to 15 LPFM images of the +/+ and oim/oim fibers were used for statistical analysis respectively.

C. Molecular dynamics (MD) simulation

To exclude the functions of mineral and compare the chain substitution induced changes of the electromechanical property of +/+ and oim/oim collagen fibrils, we simulated the electric induced displacements of chains in mineral-free heterotrimer and homotrimer models. We selected a segment of real sequences[20] (from residue Nos. 331 to 366) of type I α-1 and α-2 chains of *Mus musculus* (wild-type mouse) to generate our heterotrimeric model (heterotrimer: five-strand collagen microfibrils, each microfibril has two α-1 chains and one α-2 chain) [Fig. 2(a)] and homotrimer model (homotrimer: five-strand collagen microfibrils,[77,78] each microfibril has three α-1 chains) [Fig. 2(b)]. Both the α-1 and α-2 chains in the hetero- and homotrimer consisted of 36 amino acid residues with G-X-Y triplets. The two termini of each chain were capped by assigning the first residue to the acetylated N-terminus (ACE), and the last residue to the *N*-methylamide C-terminus (CT3). The selected residue sequences of α-1 and α-2 chains in the models for this study were (The detailed information of amino acid residue names and their charge information were given in Tables S3 and S4 in the supplementary material.) as follows:

α-1:NGARGPSGPQGPSGPPGPKGNSGEPGAPGNKGDTGAKC;
α-2:NGPRGIPGPAGAAGATGARGLVGEPGPAGSKGESGNKC.

The α-1 and α-2 chains were adapted from the NCBI protein database (http://www.ncbi.nlm.nih.gov/protein): AAH50014.1 for α-1 chain and NP_031769.2 for α-2 chain.[79] The hetero- and homotrimer were created by imitating Smith's five-strand collagen microfibrils model (PDB ID: 4CLG[78]). Mutation was done using software UCSF Chimera 1.11.2.[80] The Smith's model 4CLG comprises 5 identical collagen microfibrils [Fig. 2(e)], and each microfibril included 3 identical α-helices with 12 periodic G-P-P triplets as well as C-terminus and N-terminus. In our work, the hetero- and homotrimer comprised 6770 and 6750 atoms, respectively. The three chains of hetero-/homotrimer had the same polar direction. The atomistic simulations were performed using GROMACS[81] (version 4.5.x) package and AMBER99SB-ILDN force field.[82] The hetero- and homotrimer were solvated in a TIP3P (three-site transferrable intermolecular potential) water box[83] with dimensions of $14 \times 30 \times 14$ nm^3 with periodic boundary condition applied. Before the actual simulation, energy minimization was first conducted (see Fig. S1 in the supplementary material). After energy minimization, the hetero- and homotrimer were equilibrated to 300 K [NVT equilibration, 500 ps, V-rescale (the velocity rescale method)] with backbones restrained. Afterward, the backbones were released, but one end of the hetero- and homotrimer was restrained. The pressure was equilibrated to 1 bar (NPT equilibration, 90 ns, Parrinello-Rahman algorithm). The cutoff and PME were set to 1.0

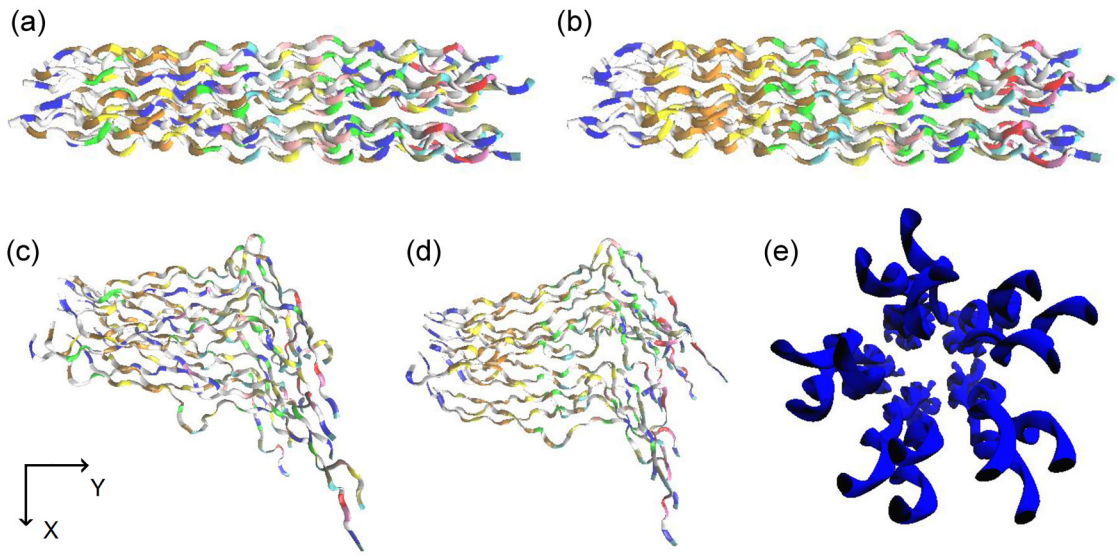

FIG. 2. The five-strand models of (a) heterotrimer and (b) homotrimer. The changes of (c) heterotrimer and (d) homotrimer models under the 3 V/nm electric field along the x direction. (e) The cross section of the five-strand Smith's collagen model.

and 4, respectively. The lengths of the heterotrimer and homotrimer models after NPT equilibrations were ∼106 Å. Afterward, water molecules were removed (vacuum) from the heterotrimer and homotrimer to exclude the electric perturbance from polar water molecules. We simulated the responses of pure collagen microfibrils (ideal models) under the electric field. To compare the in-plane and out-of-plane piezoresponses of the hetero- and homotrimer, we applied a uniform electric field (3 V/nm) in the x direction, which is perpendicular to the long axis of the fibril, as shown in Fig. 2. This simulation setup is to fit the PFM experiments. The N-terminus of each chain in the two models was fixed while the other residues were free to mimic the experimental setup (or to prevent the collagen bundle from drifting inside the simulation box). The hetero- and homotrimer were simulated through 5 ns in vacuum under the applied electric field. The cutoffs were set to 0. The software VMD[84] was used to visualize the in-plane and out-of-plane electric responses of the hetero- and homotrimer under the applied electric field. All the polypeptide chains in the two models have showed displacements along both the x and y directions (perpendicular and parallel to the long axis of the fibril) [Figs. 2(c) and 2(d)].

III. RESULTS AND DISCUSSION

A. Biopiezoelectricity of +/+ and oim/oim collagen fibers

Collagen fibers exhibit a stronger shear (in-plane) piezoresponse compared to the normal (out-of-plane) piezoresponse upon application of an electric field perpendicular to the long axis of the fiber because of the C_6 symmetry of collagen.[56,85] The representative VPFM and LPFM images of both +/+ and oim/oim collagen fibers are presented in Fig. 3. The conductive probe (PPP-CONTSCPt, Nanosensors, Switzerland) is used for PFM experiments. In the experiments, the oim/oim sample is scanned first, followed by the +/+ sample. In all of the height images shown in Fig. 3, the periodic D-space structure of type I collagen can be clearly observed, suggesting that the plane with the fibrils is parallel to the cantilever axis. The double arrows in Figs. 3(c) and 3(d) indicate the direction normal to the long axis of the fibers, which is defined as fibrillar orientations.[86] The cantilever orientation and scan direction are also marked besides Fig. 3(d). For the given fibrillar orientations here, high in-plane and low out-of-plane piezoresponses would be expected due to the stronger shear piezoelectricity of the C_6 symmetry of the collagen. As expected, the piezoresponse of either +/+ or oim/oim collagen fibers [Figs. 3(e) and 3(f)] is quite low with intrinsic VPFM amplitude (after SHO fitting) ranges of 0.33–0.54 pm and 0.35–6.65 pm, respectively, while the relative strong phase contrast [Fig. 3(i)] may be due to the cantilever buckling effect.[87] By using LPFM image, high resolution fine structures in each fiber can be revealed in height [Figs. 3(c) and 3(d)] and amplitude images [Figs. 3(g) and 3(h)]. The +/+ collagen fibers show overall stronger piezoresponse than that of the oim/oim fibers, and the morphology of the fiber in the valley regions exhibits an even stronger piezoresponse and forms regular patterns as shown in the amplitude image [Fig. 3(g)]. For the oim/oim fibers, in addition to the generally low piezoresponse, they show highly nonuniform amplitude contrast along the long axis of the fiber [Fig. 3(h)], and nearly no piezoresponse at some random regions [the darkest purple contrast in Fig. 3(h)]. The valley regions also have no stronger amplitude response in the oim/oim fibers, which indicates that the regular piezoresponse patterns observed in +/+ fibers valleys are intrinsic properties and not due to the crosstalk with the topographic information. In addition, the disappearance of regular patterns in the amplitude image [Fig. 3(h)] for the oim/oim fibers should not due to the duller

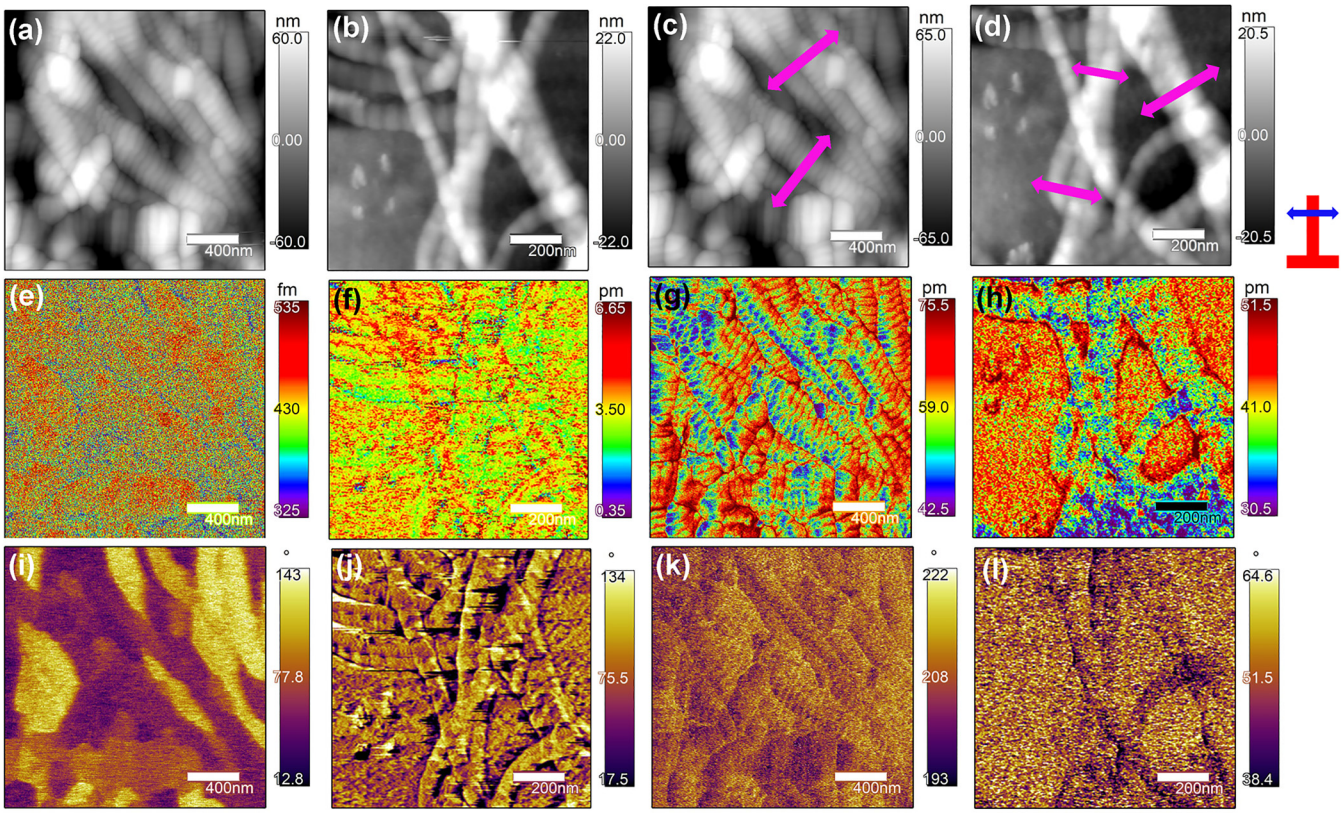

FIG. 3. Representative VPFM (1st and 2nd columns) and LPFM images (3rd and 4th columns) of the +/+ collagen fibers (1st and 3rd columns) and oim/oim collagen fibers (2nd and 4th columns). (a)–(d) Height images, [(e)–(h)] PFM amplitude images, and [(i)–(l)] PFM phase images. Please note that the scanned areas of the +/+ and oim/oim samples are the same in VPFM and LPFM experiments, respectively, and the amplitude images in VPFM are intrinsic amplitude images. The double arrow in (c) and (d) indicates the fibrillar orientation, which is normal to the long axis of the fiber. The cantilever orientation and scanning direction are marked besides (d).

tip since the oim/oim is scanned first. Furthermore, the relative weak phase contrast is observed for both +/+ and oim/oim collagen fibers in the LPFM phase images [Figs. 3(k) and 3(l)], which suggests that the variation of the tip–sample contact stiffness or the electrostatic effect can be excluded and the in-plane sectors of the polar vectors of collagen fibrils have a similar direction with each other. The +/+ collagen fibers are composed of well-developed molecules during mineralization, showing regular and periodic morphology and piezoresponse distribution, while oim/oim collagen fibers have intrinsically molecular structural defects. Although the oim/oim fibers still show periodic morphology, the intrinsic defects may cause a weak response to electric stimulation, i.e., weaker piezoresponse, and the irregular piezoresponse along the fiber.

Figure 4 shows another set of LPFM results on +/+ and oim/oim collagen fibers in different scanning sizes using different types of conductive probes (PPP-CONTPt, Nanosensors, Switzerland). Again, the oim/oim sample is scanned first, followed by the +/+ sample. From the height images [Figs. 4(a) and 4(i), scanning size: $1 \times 1\,\mu m^2$], it can be seen that the +/+ collagen fiber possesses a much larger diameter than that of the oim/oim collagen fiber. The different fiber diameter may be due to different fibril numbers in the bundle of each +/+ and oim/oim fiber. To inspect the sub-fibril level structure, we also show LPFM results on +/+ and oim/oim collagen fibers with a scanning size of $350 \times 350\,nm^2$. From the height images [Figs. 4(e) and 4(m)], the +/+ collagen fibers show the highly organized and compact structure while the oim/oim collagen fibers show the ordered but loosely packed structure. From the LPFM amplitude images [Figs. 4(b), 4(f), 4(j), and 4(n)], the oim/oim fibers show generally low piezoresponse and highly nonuniform amplitude contrast along the long axis of the fiber. In contrast, the +/+ fibers show overall stronger piezoresponse than that of the oim/oim fibers. In addition, the valley regions always exhibit a stronger piezoresponse and form regular patterns in +/+ collagen fibers. The gap and overlap regions of the +/+ collagen fibers exhibit different electromechanical amplitude values [Fig. 4(f)], which is consistent with the observation by Jiang *et al.*[59] The dramatically high amplitude along the sidewalls (dark red color) of the fibers may be due to the slippery of the tip–fiber contact. It is worthy of noting that the fibers marked by red lines in Figs. 4(e) and 4(m) almost have the same fibrillar orientation. These two

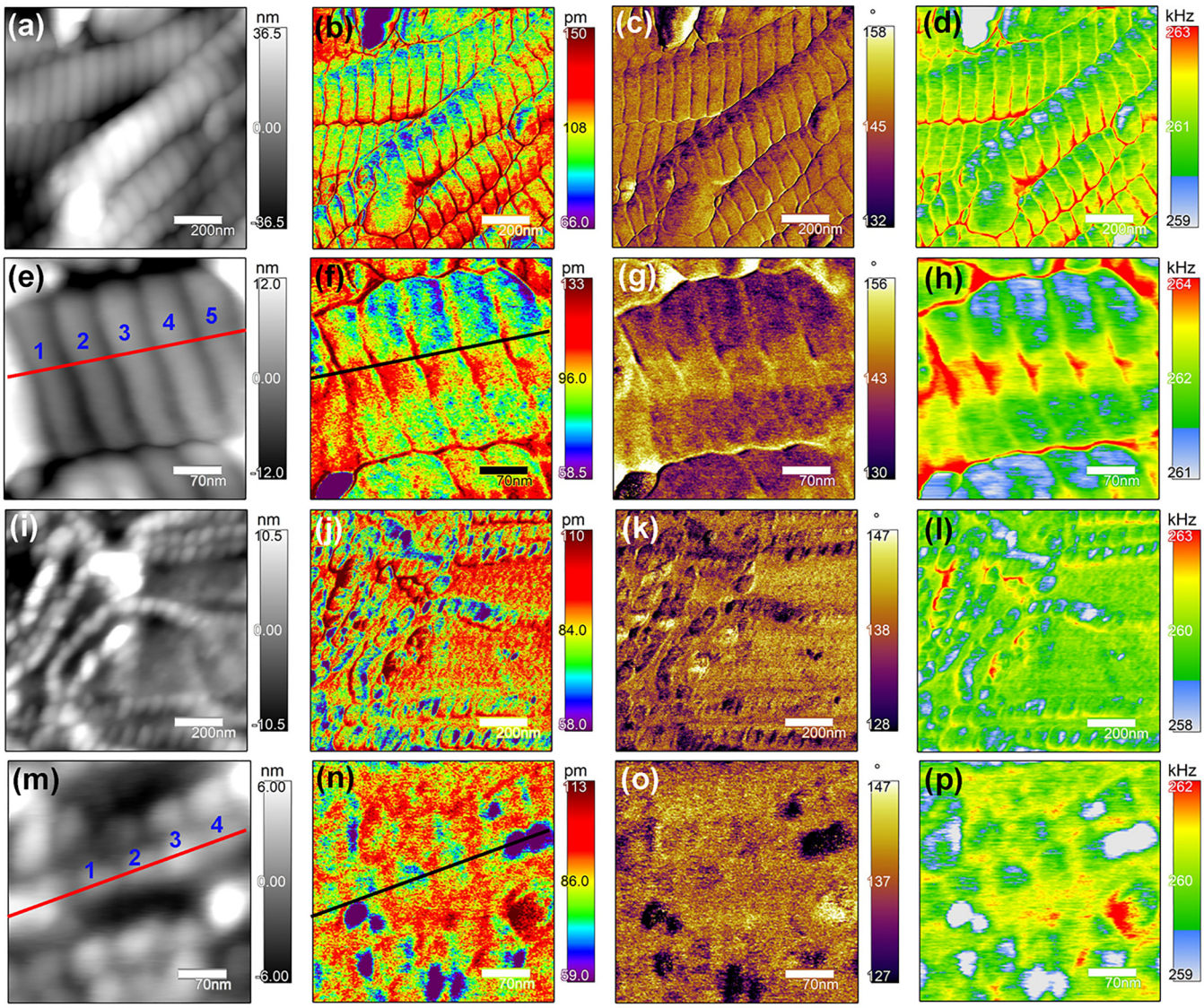

FIG. 4. Representative LPFM images of +/+ collagen fibers (1st and 2nd rows) and oim/oim collagen fibers (3rd and 4th rows). [(a), (e), (i), (m)] Height images, [(b), (f), (j), (n)] amplitude images, [(c), (g), (k), (o)] phase images, and [(d), (h), (l), (p)] contact resonance frequency images. The scanned areas are $1 \times 1\,\mu m^2$ (1st and 3rd rows) and $350 \times 350\,nm^2$ (2nd and 4th rows).

fibers are perfect examples to compare the piezoresponse between the +/+ and oim/oim fibers. The phase values in LPFM phase images [Figs. 4(g) and 4(o)] are close, indicating that the fibrillar orientation of the two fibers is similar. From Figs. 4(f) and 4(n), it is clear that the +/+ collagen fibers show a highly organized structure with regular patterned electromechanical responses while the oim/oim collagen fibers show nonuniform amplitude contrast. From the phase images [Figs. 4(c), 4(g), 4(k), and 4(o)], weak phase contrast is still observed for both +/+ and oim/oim collagen fibers, also suggesting the similar orientation of the in-plane sector of the polar vector. In addition, the smaller contrast in contact resonance frequency images [Figs. 4(d), 4(h), 4(l), and 4(p)] for both +/+ and oim/oim collagen fibers suggests that the scanned areas have a homogeneous elastic property.

Figure 5 shows the height and LPFM amplitude data profiles along the lines in the corresponding height [see Figs. 4(e) and 4(m)] and amplitude images [see Figs. 4(f) and 4(n)] of +/+ and oim/oim collagen fibers. The dramatically high piezoelectric amplitude along the sidewalls of fibers may be due to the slippery of the tip–fiber contact, and thus we analyze the data from the central region along the long axis of the fiber. Figure 5 demonstrates that the amplitude maxima are at the height valley regions

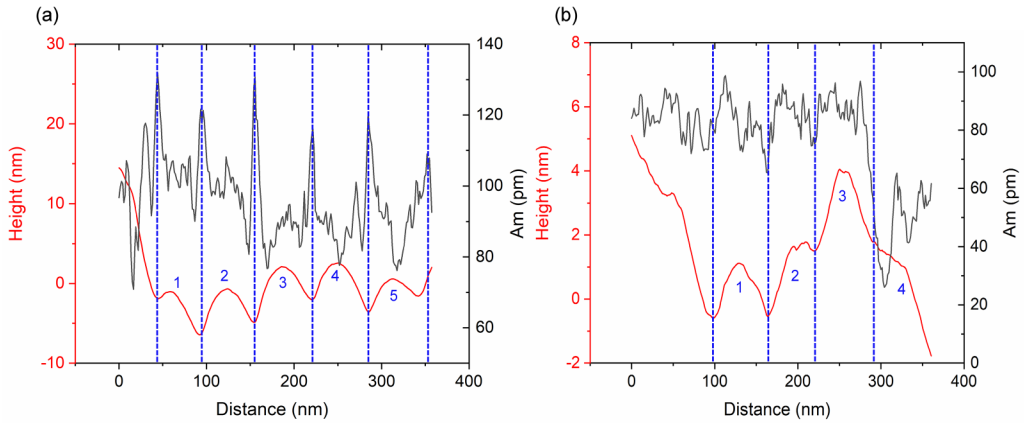

FIG. 5. Height and LPFM amplitude data profiles along the lines in the corresponding height and amplitude images of (a) +/+ collagen fiber and (b) oim/oim collagen fiber in Fig. 4.

in the +/+ collagen fiber [Fig. 5(a)]. The amplitude fluctuates in the gap and overlap zones inside a periodic unit (1, 2, 3, 4, 5). In comparison, there is no obvious correspondence between the amplitude and height in the oim/oim fiber [Fig. 5(b)]. The amplitude fluctuation in the gap and overlap zones inside each periodic unit (1, 2, 3, 4) is also observed in the oim/oim fiber. The variations in the amplitude profiles of the gap and overlap zones may indicate the compositional differences of amino acid residues inside the +/+ and oim/oim collagen fibrils. The well-organized sub-fibril structure and the periodic amplitude variation along the +/+ collagen fibers indicate that better molecular assembly and functionalization of the collagen are controlled by the heterotrimer model. Moreover, the average values of amplitude profiles along the lines are 96.4 pm and 77 pm with standard deviations of 11.5 pm and 16.4 pm for +/+ and oim/oim fibers, respectively. The +/+ fiber shows a larger in-plane piezoresponse than that of the oim/oim fiber.

We collect amplitude data from 10 to 15 LPFM images containing 30 collagen fibers to plot the box charts with the statistical values of amplitude for +/+ and oim/oim collagen fibers, respectively [Fig. 6(g)]. The LPFM images for this statistical analysis are

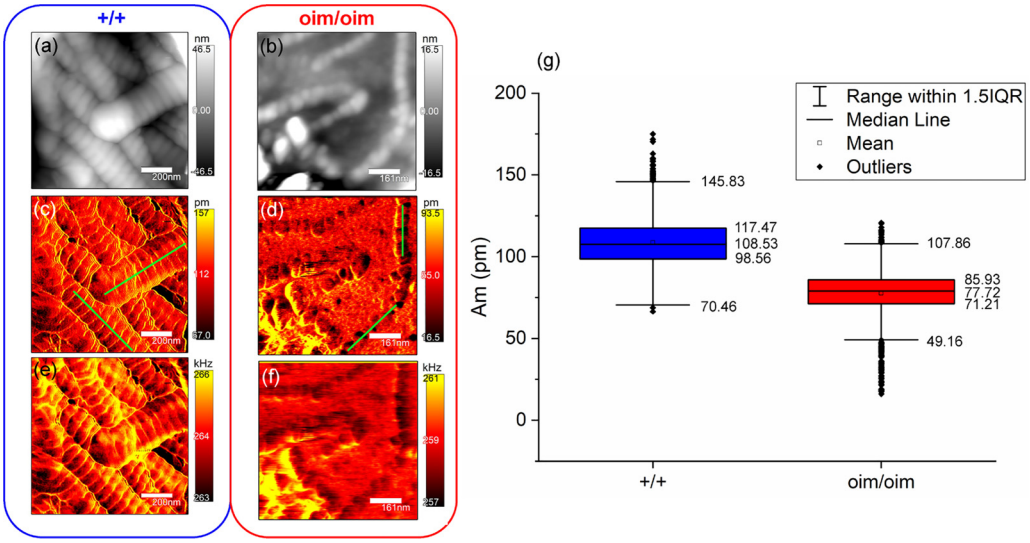

FIG. 6. More representative LPFM images of [(a), (c), (e)] +/+ collagen fibers and [(b), (d), (f)] oim/oim collagen fibers. [(a) and (b)] Height images, [(c) and (d)] amplitude images, and [(e) and (f)] contact resonance frequency images. Thirty (30) collagen fibers are chosen to plot the statistical amplitude box charts for +/+ and oim/oim collagen fibers, respectively, in (g) with 2–3 collagen fibers selected in each LPFM amplitude image. The box data for +/+ and oim/oim are collected from the central region along the long axis of the fiber as illustrated in (c) and (d).

acquired under the same experimental parameters as those adopted in the measurement of Fig. 4. In each image, amplitude data are collected from the central region along the long axis of the fiber in 2–3 fibers, as illustrated in Figs. 6(c) and 6(d). From Fig. 6(g), the mean values of LPFM amplitude are 108.53 pm and 77.72 pm with interquartile ranges (IQRs) of 98.56–117.47 pm and 71.21–85.93 pm for +/+ and oim/oim fibers, respectively. The IQR is essentially the range of the middle 50% of the data, which measures where the bulk of the values lie. From the IQR, it is observed that the 50% of the amplitude values of the +/+ fibers are larger than those of the oim/oim fibers as the lower boundary of the IQR of +/+ fibers is larger than the upper boundary of IQR of oim/oim. The ranges within 1.5 times of IQR (1.5IQR: covering more than 99% of the collected data) are 70.46–145.83 pm and 49.16–107.86 pm for +/+ and oim/oim collagen fibers, respectively. Most of the outliers for oim/oim are located below the lower range of its 1.5IQR, while most the outliers for +/+ are located over the upper range of the 1.5IQR of +/+ data. Based on those statistical analysis, the +/+ collagen fibers are demonstrated to show generally larger in-plane piezoresponses than that of the oim/oim collagen fibers. It is worthy of noting that error propagation should be carefully evaluated because the quality factor, the inverse optical lever sensitivity, and the height and length of cantilevers in the measurements are statistically different. The probes (PPP-CONTPt, Nanosensors, Switzerland) were randomly selected to replicate force curves on a silicon wafer 40 times to obtain the statistical value of the inverse optical lever sensitivity. The cantilever's nominal height is 12.5 μm with the range varied from 10 μm to 15 μm while the cantilever's nominal length is 450 μm with the range varied from 440 μm to 460 μm (manufacturer's data). 40 data points of the PFM amplitude and quality factor were measured on the +/+ and oim/oim collagen fibers, respectively. The detailed error propagation calculation procedure and typical force curve can be found in Fig. S2 of the supplementary material. The resulting lateral piezoresponse amplitude values are measured with ±18.2% and ±19.1% error for +/+ and oim/oim fibers, respectively.

By using PFM, we present the evident discrepancies of the sub-fibril level structure and electromechanical responses between the +/+ and oim/oim collagen fibers. From the PFM results and statistical analysis, larger in-plane piezoelectric responses of +/+ collagen fibers are revealed. The α-2 chain has been found to produce a significant positive effect on self-assembly and electromechanical property of type I collagen. Therefore, in addition to the previously reported mechanical and morphological changes, the differences of the in-plane structure and electromechanical property between the +/+ and oim/oim fibers could be an additional sign of osteogenesis imperfacta or brittle bone disease.

B. Chemistry changes of +/+ and oim/oim collagen fibers

Surface morphology of +/+ and oim/oim collagen fibers and atomic content of carbon (C), oxygen (O), calcium (Ca), nitrogen (N), potassium (K), and phosphorus (P) are scanned and analyzed by using the Field-emission Scanning Electron Microscope (FESEM, Sigma 300 ZEISS, Germany) equipped with an Energy-Dispersive X-ray Spectrometer (EDS, Ultimax 65, Oxford Instruments, Britain). The FESEM surface morphology images and EDS results are shown in Fig. 7. The dispersed oim/oim collagen fibers show short and bend shape compared to the straight long-stranded +/+ collagen fiber bundles [Figs. 7(a) and 7(b)]. From the EDS mappings of the elements, i.e., C, O, Ca, N, K, and P for +/+ and oim/oim collagen fibers, it can be seen that Ca and P are commonly existed in the mineral matrix [hydroxyapatite: $Ca_5(PO_4)_3(OH)$], while C, O, N, and K are usually found in the collagen. The quantitative atomic occupation analysis of each element in EDS mappings [Fig. 7(c)] reveals that the sum of atomic content of C, O, N, and K in the +/+ collagen fiber (sum: 89.62%; C: 45.45%, O: 25.89%, N: 18.14%, K: 0.14%) is larger than those of the oim/oim collagen fiber (sum: 77.91%; C: 45.63%, O: 17.89%, N: 14.39%, K: 0). While the sum of atomic content of Ca and P in the +/+ collagen fiber (sum: 0.79%; Ca: 0.79%, P: 0) is smaller than that of oim/oim collagen fiber (sum: 7.49%; Ca: 6.5%, P: 0.99%). The organic phase occupies more than the inorganic phase for collagen fibers. In addition, the mineral content in oim/oim fiber is more than that in the +/+ fiber. The change of mineral content is reasonable since bone mineral may act as a reservoir from which the inorganic ions can be continually withdrawn for the usage or deposition for storage, as dictated by homeostasis.[88,89] Based on these findings, the chain substitution is expected to influence both the collagen fibrillar organization and mineralization.

C. Simulation of the piezoelectric behaviors of hetero- and homotrimer

The density of the 90 ns NPT and the root mean square deviation (RMSD) during the last 10 ns of the NPT simulation of the two models are plotted in Figs. S3 and S4 in the supplementary material. It is found that the fluctuation of density and RMSD of the homotrimer model are larger than those of the heterotrimer model, indicating a better structural stability of the heterotrimer model. The better structural stability of heterotrimer can also be demonstrated by its smaller interaction energy and a larger number of hydrogen bonds (Figs. S5 and S6 in the supplementary material). Hydrogen bond and interaction energy are two main parameters to evaluate the structural stability of protein in MD. To analyze this in more detail, we select three chains (chains A–C) from one microfibril to plot the displacement vs time curves (Fig. 8) for both models. It is found that the chains in the heterotrimer model generally have larger electric induced in-plane and out-of-plane displacements than those in the homotrimer model. The induced in-plane and out-of-plane displacements of chain C (α-2 chain) in heterotrimer are approximately 0.2–1 nm larger than that in the chain C (α-1 chain) of the homotrimer model [Figs. 8(e) and 8(f)]. Additionally, in a large proportion of the simulation time, the α-1 chains (chains A and B) in the heterotrimer model show larger displacement than that of the α-1 chains (chains A and B) in the homotrimer model [Figs. 8(a)–8(d)], respectively. It is worthy to note that the α-1 chains (chains A and B) may exhibit different electric responses in different structures, i.e., in heterotrimer or homotrimer models. The distinct displacements of α-1 chains (chain A and B) in hetero- and homotrimer models are probably due to the different interchain hydrogen-bonding interactions[90] because of the different chain C, i.e., α-2 chain in the heterotrimer

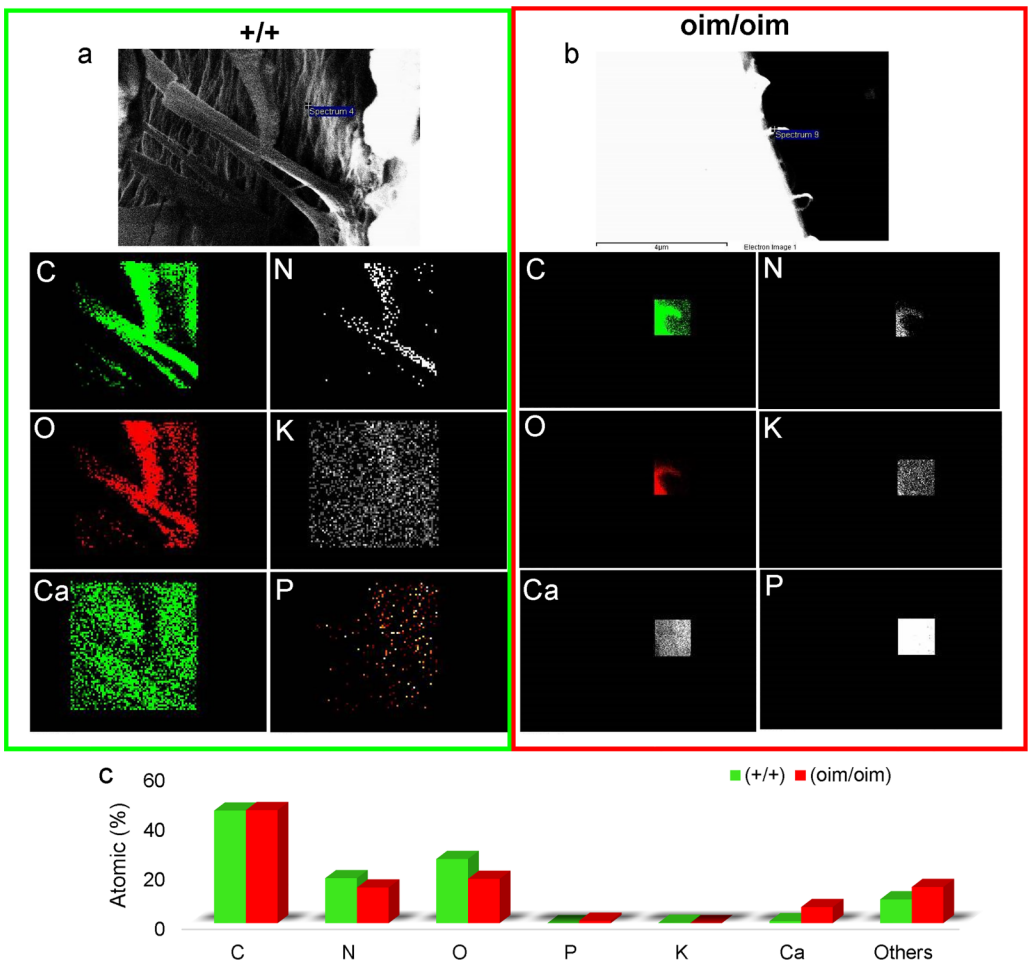

FIG. 7. FESEM images of (a) +/+ and (b) oim/oim collagen fibers, and the EDS mappings of the elements: C, O, Ca, N, K, and P in +/+ and oim/oim collagen fibers in (a) and (b), respectively. (c) The atomic occupation of each element in EDS mappings for +/+ and oim/oim collagen fibers.

model but α-1 chain in the homotrimer model. For cumulative analysis, we further plotted the root mean square fluctuation (RMSF) of all the 570 amino acid residues under the applied 3 V/nm electric field in both the hetero- and homotrimer models (Fig. 9). The residues in the heterotrimer model show generally larger fluctuations than those in the homotrimer model under the same electric field, which reveals the more piezoelectric active behavior of the heterotrimer model. Moreover, the residues in either the heterotrimer or homotrimer model exhibit larger RMSF under electric field than that without electric field. The RMSF of both heterotrimer and homotrimer is approximately 0.02–0.05 nm under zero electric field, which is much smaller than the RMSF value (0.2–0.9 nm) under the 3 V/nm electric field. The increment of the RMSF value is a convincible demonstration of the piezoelectric active behavior of the amino acids, which are consistent with the PFM measurements presented earlier.

Based on these findings, the α-2 chain is demonstrated as pivotal in stabilizing collagen structure and improving the piezoresponse of the collagen fibril. It should be noticed that the integral charge distributions of the α-1 and α-2 chains can be considered to be approximately identical (Table S4 in the supplementary material), both with positive charges located at the residue numbers (nos.) 3, 18, 30, and 36 and negative charges located at the residue nos. 23 and 32, respectively. For α-1 chain, the positively charged residues are Arg3 (no. 3)[63,79] and Lys (nos. 18, 30, and 36), while the negatively charged residues are Glu (no. 23) and Asp (no. 32). For α-2 chain, the positively charged residues are Arg3 (nos. 3 and 18) and Lys (nos. 30 and 36), and the negatively charged residues are Glu (nos. 23 and 32). The differences of the positively charged residues between α-1 and α-2 chains are Lys (α-1 chains) and Arg3 (α-2 chains) located at the residue no. 18 and negatively charged residues Asp (α-1 chains) and Glu (α-2 chains) located at the residue no. 32. This possibly indicates that increasing diversity of amino acids can improve the piezoelectric behavior of tropocollagen structures. In addition, we summarize the atomic charges of residues from α-1 and α-2 chains

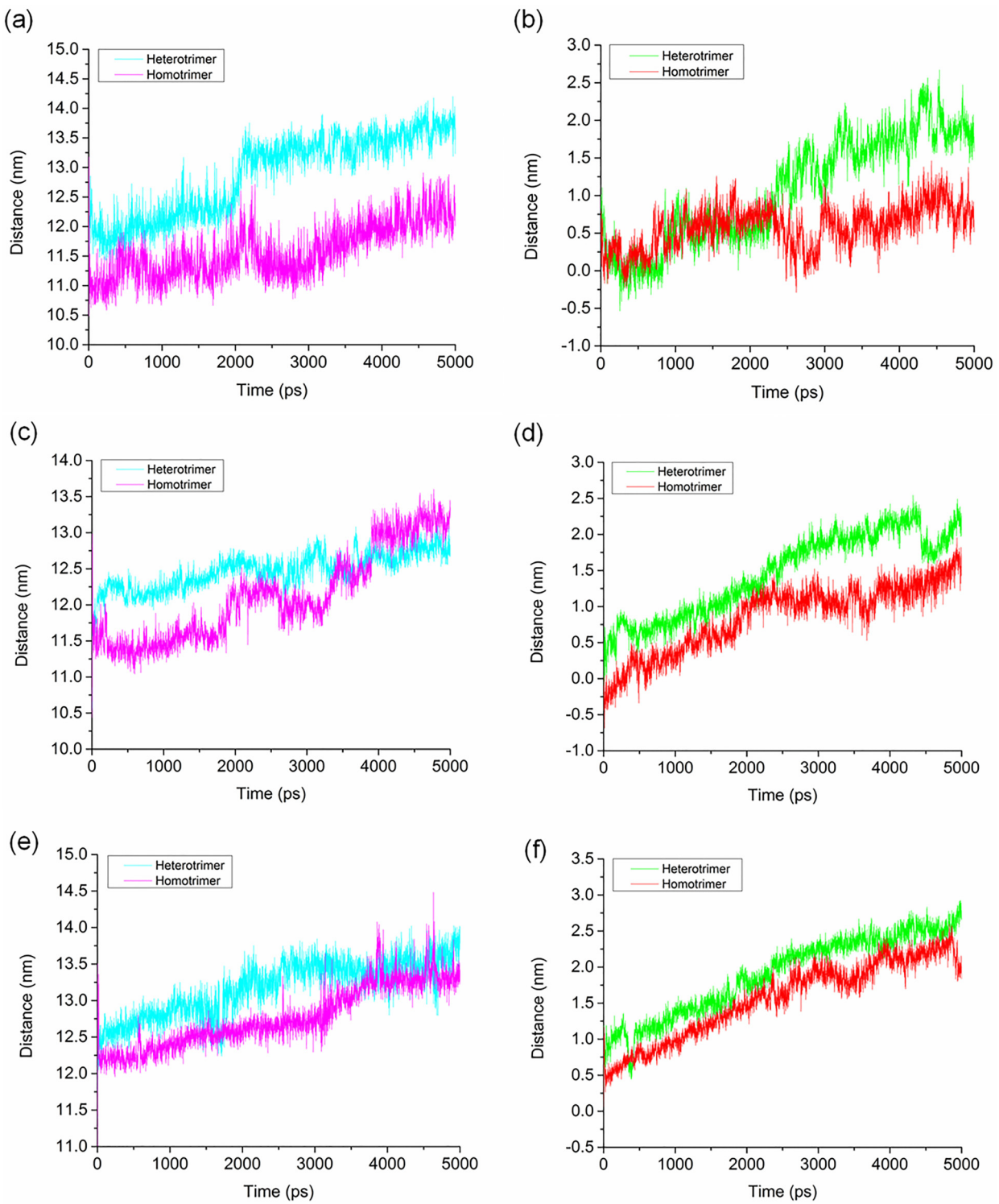

FIG. 8. The electric field induced in-plane (1st column) and out-of-plane (2nd column) displacements of [(a) and (b)] α-1 chain (chain A), [(c) and (d)] α-1 chain (chain B), and [(e) and (f)] chain C in heterotrimer (α-2 chain) and homotrimer (α-1 chain) under the 3 V/nm electric field along the x direction (shown in Fig. 2).

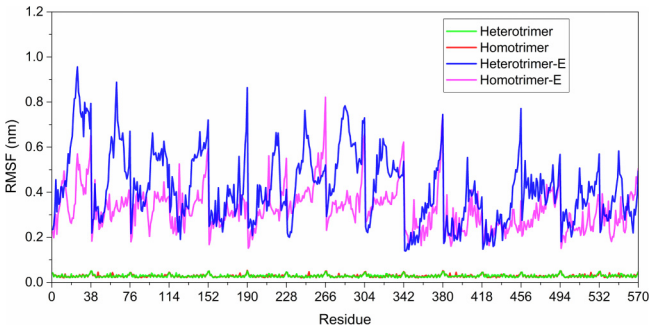

FIG. 9. Root mean square fluctuation (RMSF) plots of all of the residues in heterotrimer and homotrimer before and after applying the 3 V/nm electric fields along the x direction (shown in Fig. 2).

(excluding Gly) in the hetero- and homotrimer models (see Table S5 in the supplementary material). It is found that even the same atom can present distinct charges in different amino acids. For instance, the atoms C, O, and N (atom named according to AMBER99SB-ILDN force field) show four (4) different charges among the selected individual residues (see Table S5 in the supplementary material). The atoms HA, CA, and CB even show completely different charges in each residue. Based on these findings, it is expected that judicious increase of multiplicity of the amino acids (atomic charges) tends to produce more local electric dipoles between the adjacent chains in the oriented heterotrimeric peptide structures and thus generating stronger biopiezoelectric responses. The previously demonstrated a larger number of hydrogen bonds in heterotrimer may also be one reason for its optimized piezoelectricity. But the root cause is the existence of α-2 chain for introducing more amino acid category and atomic charges in the collagen model. Our work systematically investigates the electromechanical coupling phenomena of +/+ and oim/oim collagen fibers for the first time and hopefully provides an additional perspective for understanding the brittle bone disease. But there are still limitations since the water molecules are absent in the simulations. The effects of water molecules are ignored based on the considerations that the influences of water molecules on the collagen model depend on the water shell thickness around collagen and the residues we have chosen from the whole type I collagen model of mice. Moreover, the water molecules have unstable polarizations under the electric field,[91] which may complicate the analysis of electromechanical responses of the collagen. More future efforts are desired to address the electromechanical property of hydrated collagen under the electric field.

IV. CONCLUSION

In summary, by using PFM and molecular dynamic simulation, this study has presented the evident discrepancies of the electromechanical structure and property between the +/+ and oim/oim type I collagen fibers. The α-2 chain has been found to enhance the structural stability and electromechanical property of type I collagen. Compelling both experimental and simulation works, we thereby describe the stronger electromechanical effect by judiciously increasing the multiplicity of amino acids within the oriented heterotrimeric structure of collagen biomacromolecules. This work has provided new information about type I collagen fibers in osteogenesis imperfecta and wild-type mice bone and hopefully offer some instructions on diagnoses and treatments of human brittle bone diseases.

SUPPLEMENTARY MATERIAL

See the supplementary material (Figs. S1–S5 and Tables S1–S5) for additional results of MD simulation, including energy minimization, structural fluctuation, interaction energy, and hydrogen bond of heterotrimer and homotrimer models. Furthermore, we show the specifications of probes used in PFM experiments as well as the name, sequence, and charge of amino acids used in the MD simulation.

AUTHORS' CONTRIBUTIONS

Y.S. and T.L. contributed equally to this work.

ACKNOWLEDGMENTS

The authors would like to thank Professor Sandra Shefelbine from Northeastern University, Boston, USA and Dr. N. Rodriguez-Florez, currently at Mondragon Unibertsitatea, Spain, for the supplying of the wild-type and oim/oim bone samples. Y.S. thanks the postgraduate scholarship from National University of Singapore. Y.C. is grateful for the support from the Agency for Science, Technology and Research (A*STAR), A*STAR Computational Resource Centre, Singapore (ACRC), and National Supercomputing Centre, Singapore (NSCC). This work is supported by Ministry of Education (MOE) Singapore through National University of Singapore under Academic Research Funds (ACRF) (Nos. R-265-000-496-112 and R-265-000-596-112).

REFERENCES

[1]V. S. Bystrov, I. K. Bdikin, A. Heredia, R. C. Pullar, E. D. Mishina, A. S. Sigov, and A. L. Kholkin, in *Piezoelectric Nanomaterials for Biomedical Applications*, edited by G. Ciofani and A. Menciassi (Springer, Berlin, 2012), p. 187.
[2]E. Fukada, Nature **166**, 772 (1950).
[3]Y. Liu, H.-L. Cai, M. Zelisko, Y. Wang, J. Sun, F. Yan, F. Ma, P. Wang, Q. N. Chen, H. Zheng, X. Meng, P. Sharma, Y. Zhang, and J. Li, Proc. Natl. Acad. Sci. U.S.A. **111**, E2780 (2014).
[4]N. Amdursky, P. Beker, J. Schklovsky, E. Gazit, and G. Rosenman, Ferroelectrics **399**, 107 (2010).
[5]H. Athenstaedt, Ferroelectrics **11**, 365 (1976).
[6]E. Fukada, Q. Rev. Biophys. **16**, 59 (1983).
[7]S. B. Lang, A. A. Marino, G. Berkovic, M. Fowler, and K. D. Abreo, Bioelectrochem. Bioenerg. **41**, 191 (1996).
[8]E. Kalmykova and C. A. Mgina, Tanz. J. Sci. **38**, 209 (2012).
[9]H. R. Leuchtag and V. S. Bystrov, Ferroelectrics **220**, 157 (1999).
[10]H. Athenstaedt, Ann. N.Y. Acad. Sci. **238**, 68 (1974).
[11]Y. Tang, C. Wu, Z. Wu, L. Hu, W. Zhang, and K. Zhao, Sci. Rep. **7**, 43360 (2017).
[12]A. Marino, G. G. Genchi, E. Sinibaldi, and G. Ciofani, ACS Appl. Mater. Interfaces **9**, 17663 (2017).
[13]J. Jacob, N. More, K. Kalia, and G. Kapusetti, Inflamm. Regen. **38**, 2 (2018).

[14]S. M. Damaraju, Y. Shen, E. Elele, B. Khusid, A. Eshghinejad, J. Li, M. Jaffe, and T. L. Arinzeh, Biomaterials **149**, 51 (2017).
[15]A. H. Rajabi, M. Jaffe, and T. L. Arinzeh, Acta Biomater. **24**, 12 (2015).
[16]M. Fang and M. M. B. Holl, BoneKey Rep. **2**, 394 (2013).
[17]A. V. Persikov, J. A. M. Ramshaw, and B. Brodsky, J. Biol. Chem. **280**, 19343 (2005).
[18]C. A. G. N. Montalbetti and V. Falque, Tetrahedron **61**, 10827 (2005).
[19]C. Tkocz and K. Kühn, Eur. J. Biochem. **7**, 454 (1969).
[20]S.-W. Chang, S. J. Shefelbine, and M. J. Buehler, Biophys. J. **102**, 640 (2012).
[21]M. D. Shoulders and R. T. Raines, Ann. Rev. Biochem. **78**, 929 (2009).
[22]S. Bansode, U. Bashtanova, R. Li, J. Clark, K. H. Müller, A. Puszkarska, I. Goldberga, H. H. Chetwood, D. G. Reid, L. J. Colwell, J. N. Skepper, C. M. Shanahan, G. Schitter, P. Mesquida, and M. J. Duer, Sci. Rep. **10**, 3397 (2020).
[23]E. Beniash, Wiley Interdiscip. Rev. Nanomed. Nanobiotechnol. **3**, 47 (2011).
[24]E. Fukada and I. Yasuda, J. Phys. Soc. Jpn. **12**, 1158 (1957).
[25]H. Athenstaedt, Nature **228**, 830 (1970).
[26]S. B. Lang, Nature **224**, 798 (1969).
[27]K. Kapat, Q. T. H. Shubhra, M. Zhou, and S. Leeuwenburgh, Adv. Funct. Mater. **30**, 1909045 (2020).
[28]A. A. Marino and R. O. Becker, Nature **228**, 473 (1970).
[29]A. A. Marino, R. O. Becker, and S. C. Soderholm, Calcif. Tissue Res. **8**, 177 (1971).
[30]E. Fukada, H. Ueda, and R. Rinaldi, Biophys. J. **16**, 911 (1976).
[31]E. Korostoff, J. Biomech. **10**, 41 (1977).
[32]A. M. Ferreira, G. González, R. J. González-Paz, J. L. Feijoo, J. Lira-Olivares, and K. Noris-Suárez, Acta Microsc. **18**, 278 (2009).
[33]J. C. Góes, S. D. Figueiró, J. A. C. De Paiva, I. F. De Vasconcelos, and A. S. B. Sombra, J. Mater. Sci. Lett. **18**, 983 (1999).
[34]E. Fukada, IEEE Trans. Ultrason. Ferroelectr. Freq. Control **47**, 1277 (2000).
[35]G. Hastings, M. ElMessiery, and S. Rakowski, Biomaterials **2**, 225 (1981).
[36]J. Behari, *Biophysical Bone Behaviour: Principles and Applications* (John Wiley & Sons (Asia) Pte Ltd, Singapore, 2009).
[37]B. J. Rodriguez, A. Gruverman, A. I. Kingon, R. J. Nemanich, and O. Ambacher, Appl. Phys. Lett. **80**, 4166 (2002).
[38]A. N. Morozovska, S. V. Svechnikov, E. A. Eliseev, S. Jesse, B. J. Rodriguez, and S. V. Kalinin, J. Appl. Phys. **102**, 114108 (2007).
[39]B. J. Rodriguez, S. Jesse, S. V. Kalinin, J. Kim, S. Ducharme, and V. M. Fridkin, Appl. Phys. Lett. **90**, 122904 (2007).
[40]Y. Liu, D. N. Weiss, and J. Li, ACS Nano **4**, 83 (2010).
[41]A. Gruverman, D. Wu, B. J. Rodriguez, S. V. Kalinin, and S. Habelitz, Biochem. Biophys. Res. Commun. **352**, 142 (2007).
[42]S. Habelitz, B. J. Rodriguez, S. J. Marshall, G. W. Marshall, S. V. Kalinin, and A. Gruverman, J. Dent. Res. **86**, 908 (2007).
[43]C. Halperin, S. Mutchnik, A. Agronin, M. Molotskii, P. Urenski, M. Salai, and G. Rosenman, Nano Lett. **4**, 1253 (2004).
[44]S. V. Kalinin, B. J. Rodriguez, S. Jesse, T. Thundat, and A. Gruverman, Appl. Phys. Lett. **87**, 053901 (2005).
[45]M. Minary-Jolandan and M.-F. Yu, Appl. Phys. Lett. **97**, 153127 (2010).
[46]V. R. Binetti, J. D. Schiffman, O. D. Leaffer, J. E. Spanier, and C. L. Schauer, Integr. Biol. **1**, 324 (2009).
[47]A. Gruverman, B. Rodriguez, and S. Kalinin, J. Scann. Probe Microsc. **1**, 74 (2006).
[48]I. Bdikin, V. Bystrov, S. Kopyl, R. P. G. Lopes, I. Delgadillo, J. Gracio, E. Mishina, A. Sigov, and A. L. Kholkin, Appl. Phys. Lett. **100**, 043702 (2012).
[49]A. Heredia, V. Meunier, I. K. Bdikin, J. Gracio, N. Balke, S. Jesse, A. Tselev, P. K. Agarwal, B. G. Sumpter, and S. V. Kalinin, Adv. Funct. Mater. **22**, 2996 (2012).
[50]A. Kholkin, N. Amdursky, I. Bdikin, E. Gazit, and G. Rosenman, ACS Nano **4**, 610 (2010).
[51]Y. Liu, Y. Zhang, M.-J. Chow, Q. N. Chen, and J. Li, Phys. Rev. Lett. **108**, 078103 (2012).
[52]T. Li and K. Zeng, Acta Mater. **59**, 3667 (2011).
[53]T. Li and K. Zeng, J. Struct. Biol. **180**, 73 (2012).
[54]T. Li and K. Zeng, J. Appl. Phys. **113**, 187202 (2013).
[55]T. Li, L. Chen, and K. Zeng, Acta Biomater. **9**, 5903 (2013).
[56]C. Harnagea, M. Vallières, C. P. Pfeffer, D. Wu, B. R. Olsen, A. Pignolet, F. Légaré, and A. Gruverman, Biophys. J. **98**, 3070 (2010).
[57]M. Minary-Jolandan and M.-F. Yu, Nanotechnology **20**, 085706 (2009).
[58]M. Minary-Jolandan and M.-F. Yu, ACS Nano **3**, 1859 (2009).
[59]P. Jiang, B. Huang, L. Wei, F. Yan, X. Huang, Y. Li, S. Xie, K. Pan, Y. Liu, and J. Li, Nanotechnology **30**, 205703 (2019).
[60]Y. Cheng, L.-D. Koh, D. Li, B. Ji, M.-Y. Han, and Y.-W. Zhang, J. R. Soc. Interface **11**, 20140305 (2014).
[61]N. Zhang, Y. Cheng, X. Hu, and J. Yeo, Curr. Opin. Chem. Eng. **24**, 79 (2019).
[62]Z. Zhang, B. Liu, Y.-W. Zhang, K.-C. Hwang, and H. Gao, Carbon **77**, 1040 (2014).
[63]H. Zhan, G. Zhang, V. B. C. Tan, Y. Cheng, J. M. Bell, Y.-W. Zhang, and Y. Gu, Adv. Funct. Mater. **26**, 5279 (2016).
[64]X. Zhou, D. Li, S. Wan, Q. Cheng, and B. Ji, Acta Mech. **230**, 1413 (2019).
[65]S. Ilieva, D. Cheshmedzhieva, and T. Dudev, Phys. Chem. Chem. Phys. **21**, 16198 (2019).
[66]B. Haimov and S. Srebnik, Sci. Rep. **6**, 38341 (2016).
[67]P. V. Dolganov and V. M. Zhilin, Phys. Rev. E **87**, 062505 (2013).
[68]A. Carriero, E. A. Zimmermann, A. Paluszny, S. Y. Tang, H. Bale, B. Busse, T. Alliston, G. Kazakia, R. O. Ritchie, and S. J. Shefelbine, J. Bone Miner. Res. **29**, 1392 (2014).
[69]F. Rauch and F. H. Glorieux, Lancet **363**, 1377 (2004).
[70]R. Morello, T. K. Bertin, Y. Chen, J. Hicks, L. Tonachini, M. Monticone, P. Castagnola, F. Rauch, F. H. Glorieux, J. Vranka, H. P. Bächinger, J. M. Pace, U. Schwarze, P. H. Byers, M. Weis, R. J. Fernandes, D. R. Eyre, Z. Yao, B. F. Boyce, and B. Lee, Cell **127**, 291 (2006).
[71]K. Misof, W. J. Landis, K. Klaushofer, and P. Fratzl, J. Clin. Invest. **100**, 40 (1997).
[72]L. Imbert, J.-C. Aurégan, K. Pernelle, and T. Hoc, J. Mech. Behav. Biomed. Mater. **46**, 261 (2015).
[73]L. Imbert, J.-C. Aurégan, K. Pernelle, and T. Hoc, Bone **65**, 18 (2014).
[74]O. G. Andriotis, S.-W. Chang, M. Vanleene, P. H. Howarth, D. E. Davies, S. J. Shefelbine, M. J. Buehler, and P. J. Thurner, J. R. Soc. Interface **12**, 20150701 (2015).
[75]T. Li, S.-W. Chang, N. Rodriguez-Florez, M. J. Buehler, S. Shefelbine, M. Dao, and K. Zeng, Biomaterials **107**, 15 (2016).
[76]J. M. Wallace, B. G. Orr, J. C. Marini, and M. M. B. Banaszak Holl, J. Struct. Biol. **173**, 146 (2011).
[77]A. Barkaoui, A. Bettamer, and R. Hambli, Procedia Eng. **10**, 3185 (2011).
[78]J. M. Chen, C. E. Kung, S. H. Feairheller, and E. M. Brown, J. Protein Chem. **10**, 535 (1991).
[79]L. Ito, K. Shiraki, T. Matsuura, M. Okumura, K. Hasegawa, S. Baba, H. Yamaguchi, and T. Kumasaka, Protein Eng. Des. Sel. **24**, 269 (2011).
[80]E. F. Pettersen, T. D. Goddard, C. C. Huang, G. S. Couch, D. M. Greenblatt, E. C. Meng, and T. E. Ferrin, J. Comput. Chem. **25**, 1605 (2004).
[81]M. J. Abraham, T. Murtola, R. Schulz, S. Páll, J. C. Smith, B. Hess, and E. Lindahl, SoftwareX **1–2**, 19 (2015).
[82]K. Lindorff-Larsen, S. Piana, K. Palmo, P. Maragakis, J. L. Klepeis, R. O. Dror, and D. E. Shaw, Proteins **78**, 1950 (2010).
[83]W. L. Jorgensen, J. Chandrasekhar, J. D. Madura, R. W. Impey, and M. L. Klein, J. Chem. Phys. **79**, 926 (1983).
[84]W. Humphrey, A. Dalke, and K. Schulten, J. Mol. Graph. **14**, 33 (1996).
[85]M. R. N. A. Stapleton, T. Soulimane, and S. A. M. Tofail, *Physiological Role of Piezoelectricity in Biological Building Blocks* (Imperial College Press, London, 2016).
[86]D. Denning, S. Alilat, S. Habelitz, A. Fertala, and B. J. Rodriguez, J. Struct. Biol. **180**, 409 (2012).
[87]L. He, J. Meng, B. Zhao, J. Jiang, W. Geng, and A. Jiang, Ferroelectrics **492**, 59 (2016).

[88]R. H. Carmona, *Bone Health and Osteoporosis—A Report of the Surgeon General* (Office of the Surgeon General, US, 2004).
[89]Y. Sun, L. H. Vu, N. Chew, Z. Puthucheary, M. E. Cove, and K. Zeng, ACS Biomater. Sci. Eng. **5**, 478 (2019).
[90]R. E. Hubbard and M. Kamran Haider, *eLS* (John Wiley & Sons, Ltd, 2001).
[91]A. S. Tayi, A. Kaeser, M. Matsumoto, T. Aida, and S. I. Stupp, Nat. Chem. **7**, 281 (2015).